

UCLA

UCLA Previously Published Works

Title

Genetic, dietary, and sex-specific regulation of hepatic ceramides and the relationship between hepatic ceramides and IR [S]

Permalink

<https://escholarship.org/uc/item/64v5f1zp>

Journal

Journal of Lipid Research, 59(7)

ISSN

0022-2275

Authors

Norheim, Frode
Bjellaas, Thomas
Hui, Simon T
[et al.](#)

Publication Date

2018

DOI

10.1194/jlr.m081398

Peer reviewed



Genetic, dietary, and sex-specific regulation of hepatic ceramides and the relationship between hepatic ceramides and IR^S

Frøde Norheim,* Thomas Bjellaas,[†] Simon T. Hui,* Karthickeyan Chella Krishnan,* Jakleen Lee,* Sonul Gupta,* Calvin Pan,* Yehudit Hasin-Brumshtein,* Brian W. Parks,[§] Daniel Y. Li,^{***} Hai H. Bui,^{††} Marian Mosier,^{††} Yuping Wu,^{§§} Adriana Huertas-Vazquez,* Stanley L. Hazen,^{***} Thomas E. Gundersen,[†] Margarete Mehrabian,* W. H. Wilson Tang,^{***} Andrea L. Hevener,^{†††} Christian A. Drevon,^{†,§§§} and Aldons J. Lusis^{1,*}

Division of Cardiology* and Division of Endocrinology, Diabetes, and Hypertension,^{†††} Department of Medicine, University of California at Los Angeles, Los Angeles, CA; VITAS Analytical Services,[†] Oslo, Norway; Department of Nutritional Sciences,[§] University of Wisconsin-Madison, Madison, WI; Cleveland Clinic Lerner College of Medicine of Case Western University,^{**} Cleveland, OH; Lilly Research Laboratories,^{††} Indianapolis, IN; Department of Mathematics,^{§§} Cleveland State University, Cleveland OH; Department of Cellular and Molecular Medicine,^{***} Lerner Research Institute, Cleveland Clinic, Cleveland, OH; and Department of Nutrition,^{§§§} Institute of Basic Medical Sciences, Faculty of Medicine, University of Oslo, Oslo, Norway

ORCID ID: 0000-0001-9013-0228 (A.J.L.)

Abstract Elevated hepatic ceramide levels have been implicated in both insulin resistance (IR) and hepatic steatosis. To understand the factors contributing to hepatic ceramide levels in mice of both sexes, we have quantitated ceramides in a reference population of mice, the Hybrid Mouse Diversity Panel that has been previously characterized for a variety of metabolic syndrome traits. We observed significant positive correlations between Cer(d18:1/16:0) and IR/hepatic steatosis, consistent with previous findings, although the relationship broke down between sexes, as females were less insulin resistant, but had higher Cer(d18:1/16:0) levels than males. The sex difference was due in part to testosterone-mediated repression of ceramide synthase 6. One ceramide species, Cer(d18:1/20:0), was present at higher levels in males and was associated with IR only in males. Clear evidence of gene-by-sex and gene-by-diet interactions was observed, including sex-specific genome-wide association study results.^S Thus, our studies show clear differences in how hepatic ceramides are regulated between the sexes, which again suggests that the physiological roles of certain hepatic ceramides differ between the sexes.—Norheim, F., T. Bjellaas, S. T. Hui, K. Chella Krishnan, J. Lee, S. Gupta, C. Pan, Y.

Hasin-Brumshtein, B. W. Parks, D. Y. Li, H. H. Bui, M. Mosier, Y. Wu, A. Huertas-Vazquez, S. L. Hazen, T. E. Gundersen, M. Mehrabian, W. H. W. Tang, A. L. Hevener, C. A. Drevon, and A. J. Lusis. **Genetic, dietary, and sex-specific regulation of hepatic ceramides and the relationship between hepatic ceramides and IR.** *J. Lipid Res.* 2018. 59: 1164–1174.

Supplementary key words animal models • diabetes • lipidomics • mass spectrometry • sphingolipids • gonadectomy • sex hormones • genome-wide association studies • insulin resistance

Ceramides are bioactive sphingolipids, mainly composed of a sphingosine backbone and fatty acid chains of different lengths. They play important roles in cell biology and have been implicated in development of metabolic dysfunction, hepatic steatosis, and insulin resistance (IR) in mice (1) as well as in humans (2). Pharmacological inhibition

This work was supported by National Institutes of Health Grants HL28581, HL114437, HL30568, HL123021, P20HL113452, R01DK106000, and R01HL126827; Transatlantic Network of Excellence Award 12CVD02; Research Council of Norway Grant 240405/F20; the Johan Throne-Holst Foundation for Nutrition Research; the Freia Medical Research Foundation; and Food Biomarkers Alliance (FOODBALL) Project Number 246413/E50. The content is solely the responsibility of the authors and does not necessarily represent the official views of the National Institutes of Health. T.B., T.E.G., and C.A.D. are affiliated with VITAS Analytical Services. VITAS Analytical Services is a contract laboratory providing chromatographic analytical services.

Manuscript received 24 October 2017 and in revised form 30 March 2018.

Published, *JLR Papers in Press*, May 8, 2018
DOI <https://doi.org/10.1194/jlr.M081398>

Abbreviations: *Cers*, ceramide synthase; Dcc, deleted in colorectal cancer; GDR, glucose disposal rate; GIR, glucose infusion rate; HF/HS, high-fat/high-sucrose; HGP, hepatic glucose production; HMDP, Hybrid Mouse Diversity Panel; HOMA-IR, homeostatic model assessment of insulin resistance; IR, insulin resistance; LD, linkage disequilibrium; MRM, multiple reaction monitoring; Neto1, neuropilin and toll-like 1; qPCR, quantitative PCR; TAG, triacylglycerol.

The data discussed in this publication have been deposited in NCBI's Gene Expression Omnibus (Norheim et al., 2018) and are accessible through GEO Series accession number GSE64770 (<http://www.ncbi.nlm.nih.gov/geo/query/acc.cgi?acc=GSE64770>).

¹To whom correspondence should be addressed.

e-mail: JLusis@mednet.ucla.edu

^SThe online version of this article (available at <http://www.jlr.org>) contains a supplement.

Copyright © 2018 by the American Society for Biochemistry and Molecular Biology, Inc.

of ceramide synthesis using myriocin ameliorates saturated-fat-induced IR in rodents (3), and altered key enzymes in the ceramide biosynthetic pathway have been shown to affect hepatic steatosis and insulin sensitivity in male mice. Increased ceramide degradation by overexpressing acid ceramidase in liver and adipose tissue of male mice prevented high-fat diet-induced hepatic steatosis and improved insulin function (4). In particular, Cer(d18:1/16:0) appears to impair insulin-stimulated Akt activation (5, 6). Liver-specific or whole-body knockout mice for ceramide synthase (*Cers*)6 (the enzyme responsible for *N*-acylation of a sphingosine backbone into dihydroceramides with 16 carbon acyl-chains) exhibited reduced Cer(d18:1/16:0) levels and were protected against diet-induced IR (5). Moreover, heterozygous *Cers2* knockout mice exhibited elevated Cer(d18:1/16:0) levels and experienced hepatic steatosis and IR as compared with wild-type mice (6). Whether differences in hepatic ceramide metabolism contribute to metabolic disorders and diabetes are unclear. Furthermore, the effects of ceramides on insulin action have not been reported in females.

In the present study, we examined hepatic lipids in about 100 genetically diverse inbred strains of mice called the Hybrid Mouse Diversity Panel (HMDP). The mice were fed a high-fat/high-sucrose (HF/HS) diet for 8 weeks, promoting IR phenotypes markedly differing among the strains (7). We identified large sex differences in genetic, hormonal, and dietary regulation of hepatic Cer(d18:1/16:0), Cer(d18:1/18:0), and Cer(d18:1/20:0) ceramides, suggesting that different ceramides play different roles in males and females.

RESEARCH DESIGN AND METHODS

Animals

All the mouse strains included in the HMDP study were obtained from the Jackson Laboratory and have been described in detail (8). The experimental design of the HF/HS feeding study has been described previously (7). Briefly, the mice were maintained on a chow diet (Ralston Purina Company) until 8 weeks of age before switching to a HF/HS (Research Diet-D12266B, New Brunswick, NJ) diet for 8 weeks. The gonadectomy and ovariectomy studies are described in detail elsewhere (9). The mice were either maintained on chow diet for 16 weeks or on chow diet until 8 weeks of age, or then switched to a HF/HS diet for 8 weeks. The mice were gonadectomized or sham operated under isoflurane anesthesia at 6 weeks of age. Mice from both studies were euthanized after 4 h fasting starting between 10.30 AM and noon.

Our study was performed in strict accordance with the recommendations in the *Guide for the Care and Use of Laboratory Animals* of the National Institutes of Health. All animals were handled according to approved institutional animal care and use committee protocols (#92-169) of the University of California at Los Angeles. The procedures for handling animals were approved by the Institutional Care and Use Committee at University of California, Los Angeles.

Murine liver lipid extraction and quantification

Murine liver samples (about 20 mg) from 271 female and 268 male livers were homogenized and lipids extracted by 10 vol of chloroform:methanol (v:v 2:1) (10). The organic fraction was

subsequently analyzed on the untargeted lipidomics platform. One to four livers were included per sex and strain depending on accessibility. In addition, a selection of mouse livers ($n = 18$) from five different strains of mice (A/J, BALB/cJ, C3H/HeJ, C57BL/6J, and DBA/2J) were chosen for more detailed structural characterization of the endogenous ceramides using a targeted lipidomics platform. Semi-quantification of the lipids was performed by using class-specific exogenous internal standards. The exogenous ceramide, Cer(d18:1/12:0), was used as a class-specific internal standard for ceramides, and was added to the murine and bovine liver homogenates prior to the Folch extraction. The main function of the class-specific internal standards was to normalize the lipid response prior to statistical analysis. The quality control samples were analyzed alongside the murine liver samples (for every tenth sample). The coefficients of variation for Cer(d18:1/16:0), Cer(d18:1/18:0), and Cer(d18:1/20:0) were better than 14, 14, and 10%, respectively. Measurements of total triacylglycerol (TAG) using a colorimetric assay (Sigma-Aldrich, St. Louis, MO) were performed as previously described (11).

Untargeted lipidomics analyses on murine livers

Untargeted comprehensive lipidomics analyses were performed on sample and quality control liver extracts using HPLC coupled to TOF-MS. This platform allows determination of glycerolipids, glycerophospholipids, cardiolipins, sphingolipids, free fatty acids, and cholesterol esters. In total, 262 specific lipids within these classes were identified. A 1260 Agilent chromatographic system comprising an autosampler, a binary pump, and a TCC column heater unit coupled to a TOF mass spectrometer with an Agilent JetStream ionization module for enhanced sensitivity was used and operated in both positive and negative ionization mode. To obtain high-resolution chromatographic separation of the lipids, a C18-XB Kinetex analytical column with (2.1 × 150 mm, 2.6 μm) was used with a flow rate of 0.8 ml/min. The eluting mobile phase was generated using A (10:90 v/v, acetonitrile:10 mmol/l ammonium formate) and B (70:25:5 v/v, isopropanol:acetonitrile:10 mM ammonium formate) mixed by a gradient as follows: 0 min (50% B), 12 min (70% B), 55 min (100% B), 65% (100% B). Injected volume was 5 μl (positive mode) and 10 μl (negative mode). The strain names and numbers of HMDP mice used for untargeted lipidomics are listed in supplemental Table S1.

Targeted ceramide lipid analyses

Highly sensitive, targeted, and detailed ceramide analyses were performed on a selection of mouse liver extracts ($n = 18$) from five different strains of mice (A/J, BALB/cJ, C3H/HeJ, C57BL/6J, and DBA/2J) using HPLC coupled to LC-MS/MS. An identical HPLC instrumentation, as described for untargeted comprehensive lipidomics analyses, was combined with a tandem mass spectrometer with an Agilent JetStream ionization module, operated in negative mode. The same analytical column and chromatographic parameters were used to achieve identical retention times for ceramides, as observed in the untargeted lipidomics. The targeted analyses were performed in negative multiple reaction monitoring (MRM) mode. The MRM transitions were selected to distinguish ceramides with C18:1 and C18:0 sphingosine backbones. Model ceramide standards, Cer(d18:1/6:0) and Cer(d18:0/6:0), used for investigating fragmentation pattern were obtained from Sigma-Aldrich. To identify hepatic ceramides, fragmentation patterns of ceramide standards were investigated, and highly specific MRM transitions were identified. In negative ionization mode, a specific fragment B was related to the fatty acyl moiety of the ceramide structure (supplemental Fig. S1) (12). For the ceramides shown in supplemental Fig. S1 [Cer(d18:1/6:0)], a strong signal at m/z 140.1 indicates a C6:0 acyl group. The signal depicted is the mother ion [M-H]. The mass difference between A and B (A – B)

identifies the type of backbone in the ceramide structure. Based on these experiments using reference standards, we selected eight specific MRM transitions tailored to quantify the ceramides listed in supplemental Table S2. Targeted analysis showed the presence of all the examined ceramides [Cer(d18:1/16:0), Cer(d18:1/18:0), Cer(d18:1/20:0), and Cer(d18:1/22:0)] (supplemental Fig. S2A, B). We could not detect C18:0 sphingosine backbones in any of the investigated hepatic ceramides.

Plasma insulin, glucose, and lipids

Blood was collected from mice using retro-orbital bleeding under isoflurane anesthesia. Plasma levels of insulin, glucose, and LDL were measured as reported previously (13). Homeostatic model assessment of IR (HOMA-IR) was calculated using the equation [(glucose × insulin)/405].

RNA isolation and global gene expression analyses

Hepatic RNA was isolated after homogenization in Qiazol and running miRNeasy columns (Qiagen, Valencia, CA) (14). RIN values were monitored with a bioanalyzer. Global gene expression in livers from the HMDP strains was analyzed using Affymetrix HT_MG430A arrays, and data were filtered (8). For the gonadectomy study, three replicate samples per condition were sequenced to an average coverage of 21.5 million reads per sample. RNA libraries were prepared using TrueSeq kits and standard Illumina protocol for stranded sequencing. Libraries were assigned across lanes to avoid having all biological replicates on the same lane, and sequenced using 50 bp paired-end reads (six samples per lane). We aligned data to the reference mouse genome (mm10) using STAR aligner v2.5.1 (15). GENCODE transcriptome version M11 (<https://www.genecodegenes.org/>) was used in genome indexing to facilitate mapping accuracy and splice junction identification. For all samples, >90% (91–97%) of the reads aligned, of which 87% (82–91%) on average mapped uniquely. Transcript assembly and quantification were performed using Cufflinks v2.2.1 on the University of California, Los Angeles computing cluster.

Western blotting

Western blotting was performed as described previously (16). Briefly, murine liver samples were lysed in whole cell extraction buffer containing 62.5 mM Tris-HCl (pH 6.8), 2% (w/v) sodium dodecyl sulfate, and 10% glycerol, and protein content was measured using a BCA protein assay kit (Pierce). Samples were denatured in 4× LDS loading buffer (Life Technologies) with 1% 2-mercaptoethanol (Sigma-Aldrich) at 99°C for 10 min. Fifty microgram samples were loaded at 10 µl/well into 4–12% Bis-Tris gels (Invitrogen) and separated out at 130 volts for 2 h. Protein was then transferred to PVDF membranes (Immobilon) for 1.5 h at 35 V. Following transfer, membranes were washed with TBST, and then blocked in 5% skim milk (Gibco) in TBST for 1 h at room temperature. Membranes were then placed in primary antibodies on a shaker overnight at 4°C. Primary antibodies were used as follows: mouse monoclonal LASS6 (*Cers6*) (Abcam ab77603, 1:500) and rabbit monoclonal β-actin (Cell Signaling 4967S, 1:1,000). The following day, membranes were washed three times in TBST and then placed in secondary antibodies (1:2,000) for 1 h at room temperature. Blots were then washed three times in TBST and placed in Amersham ECL detection solution (GE Health Sciences). Blots were imaged using a Bio-Rad Gel-Doc imager.

Real-time quantitative PCR

Quantitative (q)PCR was carried out using a KAPA SYBR Fast qPCR kit (Kapa Biosystems), as recommended by the manufacturer. The following primer sequences were used to analyze the

mRNA levels of: *Cers6* (forward 5′→3′: CCCTTACCAGCCACTCACAG; reverse 5′→3′: GTCCTCCGGTCATCCTTGG) and *B2M* (forward 5′→3′: TACGTAACACAGTTCACCCGCCTC; reverse 5′→3′: GCAGGTTCAAATGAATCTTCAGAGCATC). Samples were run on a LightCycler 480 II (Roche) and analyzed using the Roche LightCycler 1.5.0 software. *Cers6* mRNA expression was normalized to the housekeeping gene, *B2M*, and mRNA expression and quantified using the ΔΔCt method.

Hyperinsulinemic-euglycemic clamps

Two weeks after the glucose tolerance test, dual catheters were surgically placed in the right jugular vein and glucose clamp measurements were performed on female mice 3 days after surgery (17, 18). All animals were fasted for 6 h prior to the clamp and studied in a conscious state. Basal glucose turnover was determined following a 90 min constant infusion of (5.0 µCi/h, 0.12 ml/h) with [³H]D-glucose (Perkin Elmer). After the basal period, glucose (50% dextrose; Abbott Laboratories) and insulin (8 mU·kg⁻¹·min⁻¹; Novo Nordisk Pharmaceutical Industries) plus tracer (5.0 µCi/h) infusions were initiated simultaneously, and glucose levels clamped at euglycemia (~120 mg/dl) measuring a variable glucose infusion rate (GIR). At steady state the total glucose disposal rate (GDR), measured by tracer dilution technique, is equal to the sum of the rate of endogenous or hepatic glucose production (HGP) and the exogenous (cold) GIR (17–19). The insulin-stimulated component of the total GDR is equal to the total GDR minus the basal glucose turnover rate.

Association analysis

Genotypes for all the mouse strains were obtained from the Jackson Laboratory using the Mouse Diversity Array (20). SNPs that had poor quality or had a minor allele frequency of less than 5% and a missing genotype rate of less than 10% were removed. After filtering, 200,000 SNPs were left. Genome-wide association of hepatic ceramides was performed using Factored Spectrally Transformed Linear Mixed Models, which uses a linear mixed model to correct for population structure (21). A cut-off value for genome-wide significance was set at 3.46×10^{-6} , as determined previously for the HMDP (8). Linkage disequilibrium (LD) was determined by calculated pairwise r^2 SNP correlations for each chromosome. Approximate LD boundaries were determined by visualizing $r^2 > 0.8$ correlations in MATLAB (MathWorks).

Accession number

The NCBI Gene Expression Omnibus accession number for the microarray data reported in this paper is GSE64770.

Statistics

Correlations were calculated with biweight midcorrelations. Unless otherwise noted, values are expressed as mean ± SEM. The two-sample Student's *t*-test was used to examine the difference between the two groups. One-way ANOVA was used for multiple group comparisons. All analyses were performed using R 3.1.0 (Vienna, Austria), and *P* values <0.05 were considered statistically significant.

RESULTS

Genetic and sex-specific regulation of hepatic ceramide levels

To characterize sexual dimorphisms among different liver lipid species, we measured the hepatic relative levels of different glycerolipids, glycerophospholipids, cardiolipins,

sphingolipids, free fatty acids, and cholesterol esters using untargeted lipidomics in 98 female and male inbred strains fed a HF/HS diet for 8 weeks. In total, 220 specific lipids within these classes were identified in more than 50% of the strains. **Figure 1A** shows the correlation between lipids in males and females. Most lipids showed a positive correlation between the sexes (Fig. 1A). However, the glycerophospholipids generally showed stronger correlation between the sexes than the other lipid species. Comparing the relative levels of hepatic lipids between females and males revealed large sex differences (Fig. 1B). After Bonferroni correction, 97 hepatic lipids demonstrated sexual dimorphic levels; 57 and 39 lipids were prominent in male and female livers, respectively. A large proportion of the sphingolipid species exhibited higher amounts in female than male livers, e.g., Cer(d18:1/16:0) (\log_2 fold difference: 0.69 and P value: 7.45×10^{-19}) and Cer(d18:1/18:0) (\log_2 fold difference: 1.54 and P value: 1.76×10^{-40}). However, the relative levels of hepatic Cer(d18:1/20:0) were higher in males than in females (\log_2 fold difference: 0.42 and P value: 2.93×10^{-9}). Figure 1C shows the relative levels of Cer(d18:1/18:0) in each of the 98 strains of mice.

The sphingosine backbone in ceramides consists of 18 carbons and one double bond (C18:1). Ceramides, such as Cer(d18:1/16:0) and Cer(d18:0/16:1), have identical mass and are thus indistinguishable by mass alone. Some fragmentation of ions may occur due to collision-induced dissociation as ions enter the mass spectrometer. This soft fragmentation effect was observed with ceramides identified during untargeted lipidomics analyses. In addition to the accurate mass of the identified ceramides, an ion of m/z

264 was observed. This strongly implies a sphingosine backbone moiety, which is a known fragment ion of ceramides analyzed in positive ionization mode. This was further confirmed by targeted lipidomics using LC-MS/MS where we did not detect C18:0 sphingosine backbones in any of the hepatic ceramides (see Research Design and Methods section). We found strong correlations between ceramides monitored with the targeted as well as the untargeted method (supplemental Fig. S3). This made us confident that the Cer(d18:1/16:0), Cer(d18:1/18:0), and Cer(d18:1/20:0) ceramides detected with untargeted lipidomics were Cer(d18:1/16:0), Cer(d18:1/18:0), and Cer(d18:1/20:0) ceramides, respectively. The strong correlations between ceramides of the same strain monitored with the targeted as well as the untargeted method (supplemental Fig. S3) supported our untargeted analyses. Using the targeted approaches, all females from five different strains had higher relative abundances of hepatic Cer(d18:1/16:0) (supplemental Fig. S4A) and Cer(d18:1/18:0) ceramides (supplemental Fig. S4B) than the males. Merging data from the five strains resulted in significant differences between the sexes in Cer(d18:1/16:0) ($P = 2.5 \times 10^{-6}$) and Cer(d18:1/18:0) ($P = 2.7 \times 10^{-7}$) hepatic ceramide concentrations (Fig. 1D–F).

Hepatic ceramides in relation to insulin sensitivity

We investigated the associations between hepatic Cer(d18:1/16:0), Cer(d18:1/18:0), and Cer(d18:1/20:0) ceramides and body fat percent, hepatic TAG, plasma insulin, plasma glucose concentration, and HOMA-IR. Hepatic Cer(d18:1/16:0) concentration showed a significant positive

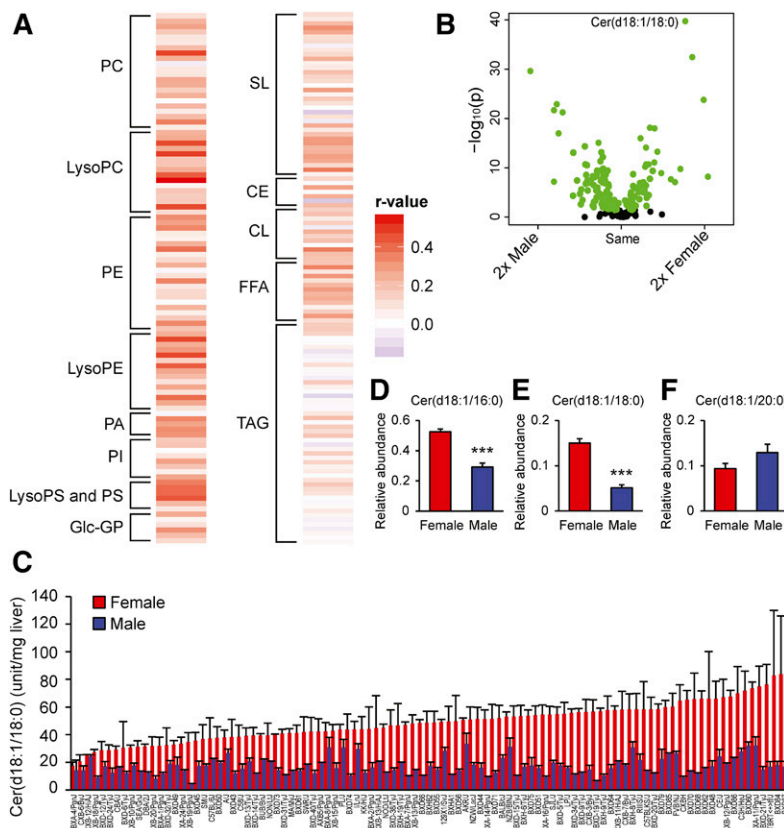


Fig. 1. Sex differences in hepatic lipid levels. Heat map showing associations in hepatic lipid levels between 98 male and female mouse strains measured with untargeted lipidomics (A). Volcano plot shows statistical significance ($-\log_{10} P$ value) versus fold change (\log_2) between the sexes for different hepatic lipid species (B). Green circles show significant differences between sexes using unpaired two-tailed Student's t -tests. Black circles show no differences between the sexes. Hepatic Cer(d18:1/18:0) (C) in female (red) and male (blue) mice ($n = 98$ strains of mice). Hepatic Cer(d18:1/16:0), Cer(d18:1/18:0), and Cer(d18:1/20:0) ceramides (D) from female and male mice (A/J, BALB/cJ, C3H/HeJ, C57BL/6J, and DBA/2J) measured with targeted lipidomics ($n = 9$ per sex). Data represent mean \pm SEM; r -value, bidweight midcorrelation; p , P value. PC, phosphatidylcholine; LysoPC, lysophosphatidylcholine; PE, phosphatidylethanolamine; LysoPE, lysophosphatidylethanolamine; PA, phosphatidic acid; PI, phosphatidylinositol; PS, phosphatidylserine; LysoPS, lysophosphatidylserine; Glc-GP, glycosylglycerophospholipid; SL, sphingolipid; CE, cholesterol ester; CL, cardiolipin. The lipids in A–C were measured with HPLC coupled to TOF-MS, and the lipids in D–F were measured with HPLC coupled to LC-MS/MS.

correlation with hepatic TAG and HOMA-IR in both males and females (Fig. 2A). However, Cer(d18:1/16:0) concentrations showed a significant positive correlation with plasma insulin in male mice only. In contrast, Cer(d18:1/16:0) exhibited a positive correlation with plasma glucose concentration in female mice, but not in males. Liver Cer(d18:1/20:0) showed positive correlations with hepatic TAG, HOMA-IR, and plasma insulin concentration only in males, suggesting sex-specificity (Fig. 2A).

To study sex-differences in IR, we plotted (volcano plot) HOMA-IR for females as compared with male mouse strains (Fig. 2B). All male strains showed a tendency toward or significantly increased HOMA-IR values compared with their female counterparts (Fig. 2B). We have previously shown that the differences in HOMA-IR among C57BL/6J, A/J, and DBA/2J male mice are inversely correlated to both whole-body and hepatic insulin sensitivity, as measured with hyperinsulinemic-euglycemic clamp (9). To investigate to determine whether HOMA-IR corresponded to whole-body and hepatic insulin sensitivity in female strains as well, C57BL/6J, A/J, and DBA/2J mice were fed a HF/HS

diet for 8 weeks and IR was assessed by hyperinsulinemic-euglycemic clamp following a 6 h fast. GIR (Fig. 2C) is supposed to reflect whole-body insulin sensitivity, and the percent insulin suppression of HGP (Fig. 2D) reflects hepatic insulin sensitivity. Comparisons of whole-body and hepatic insulin sensitivity across strains were consistent with the HOMA-IR measurements in female mice (Fig. 2E), and previous findings in males showing that A/J mice are more insulin sensitive than C57BL/6J and DBA/2J (9).

Effect of a HF/HS diet on hepatic ceramides

To study the effect of a HF/HS diet on hepatic ceramides in both sexes, we fed age-matched mice (C3H/HeJ, C57BL/6J, and DBA/2J) either a HF/HS or chow diet for 8 weeks. Mice of both sexes fed a HF/HS diet had higher relative levels of hepatic TAG (Fig. 3A–C) and tended to have increased HOMA-IR (Fig. 3D–F). The HF/HS diet did not have a large effect on hepatic Cer(d18:1/16:0) in either sex (Fig. 3G–I), although C57BL/6J females (Fig. 3H) and DBA/2J males (Fig. 3I) showed higher relative levels

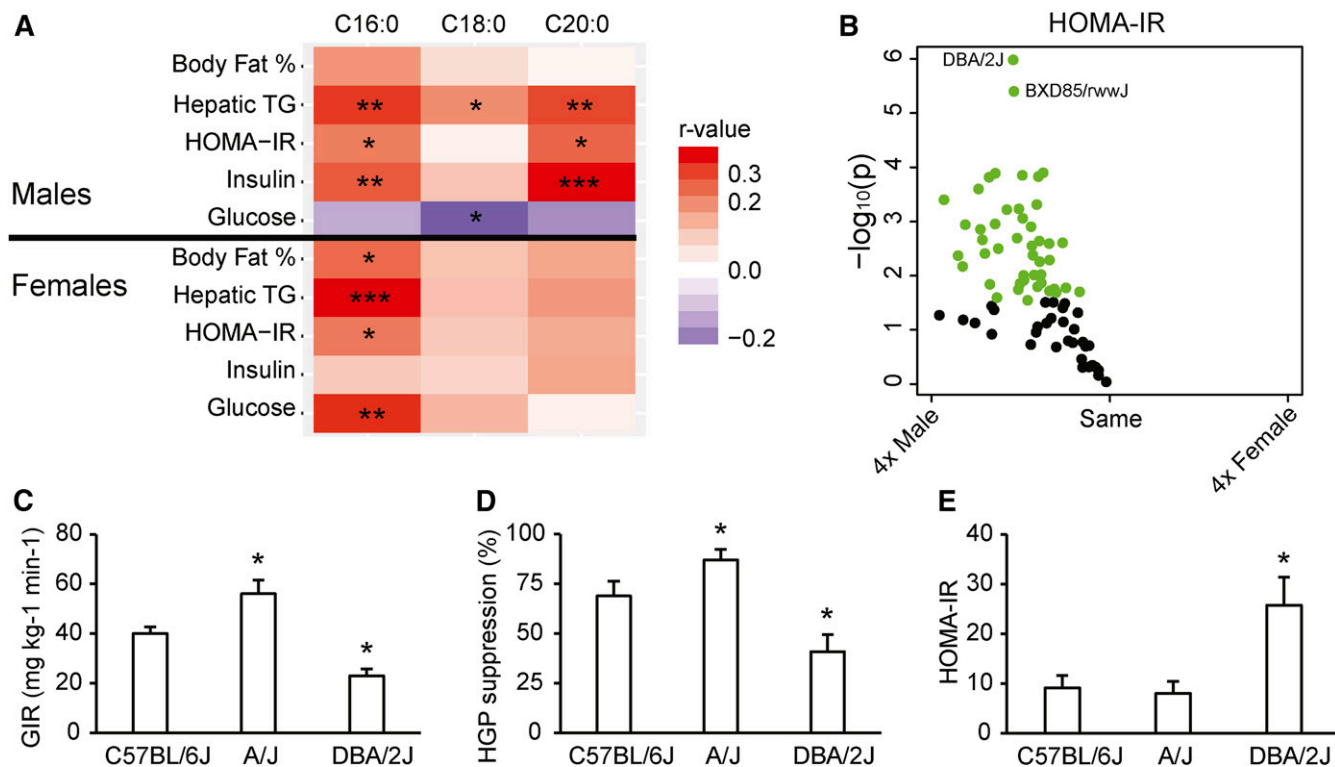


Fig. 2. Ceramides and whole-body and hepatic insulin sensitivity in mice. Heat map showing associations between hepatic ceramides and IR-related phenotypes in both sexes of 78–98 strains (A). The variation in number of strains included in the correlation analysis for the different phenotypes is caused by the fact that not all the strains have been phenotyped for plasma measurements in the HMDP. The color code represents bidweight midcorrelation between the ceramides and different phenotypes. The x axes denote the fatty acid chain of the ceramides. The darker the color, the stronger are the correlations. Volcano plots show statistical significance ($-\log_{10} P$ value) versus fold change (\log_2) between the sexes in HOMA-IR (B) ($n = 78$ strains of mice) after 8 weeks on the HF/HS diet. Green circles indicate significant difference between the sexes using unpaired two-tailed Student's *t*-tests. Whole-body (C) and hepatic insulin sensitivity (D) in C57BL/6J, A/J, and DBA/2J female mice fed a HF/HS diet for 8 weeks assessed with hyperinsulinemic-euglycemic clamp ($n = 6$ –8 per group; 4.5–5 months of age). The GIR, the amount of exogenous glucose required to maintain euglycemia during constant insulin infusion ($8 \text{ mU} \cdot \text{kg}^{-1} \cdot \text{min}^{-1}$), reflects whole-body insulin sensitivity. The HGP suppression (%) is a tracer-determined value reflecting the difference between basal glucose turnover rate and rate of HGP during hyperinsulinemia. HOMA-IR (E) in C57BL/6J, A/J, and DBA/2J female mice fed a HF/HS diet for 8 weeks ($n = 3$ –8 per strain). Values are expressed as mean \pm SEM. * $P < 0.05$, ** $P < 0.01$, *** $P < 0.001$. *Significant difference compared with C57BL/6J in the hyperinsulinemic-euglycemic clamp. The ceramides were measured with HPLC coupled to TOF-MS.

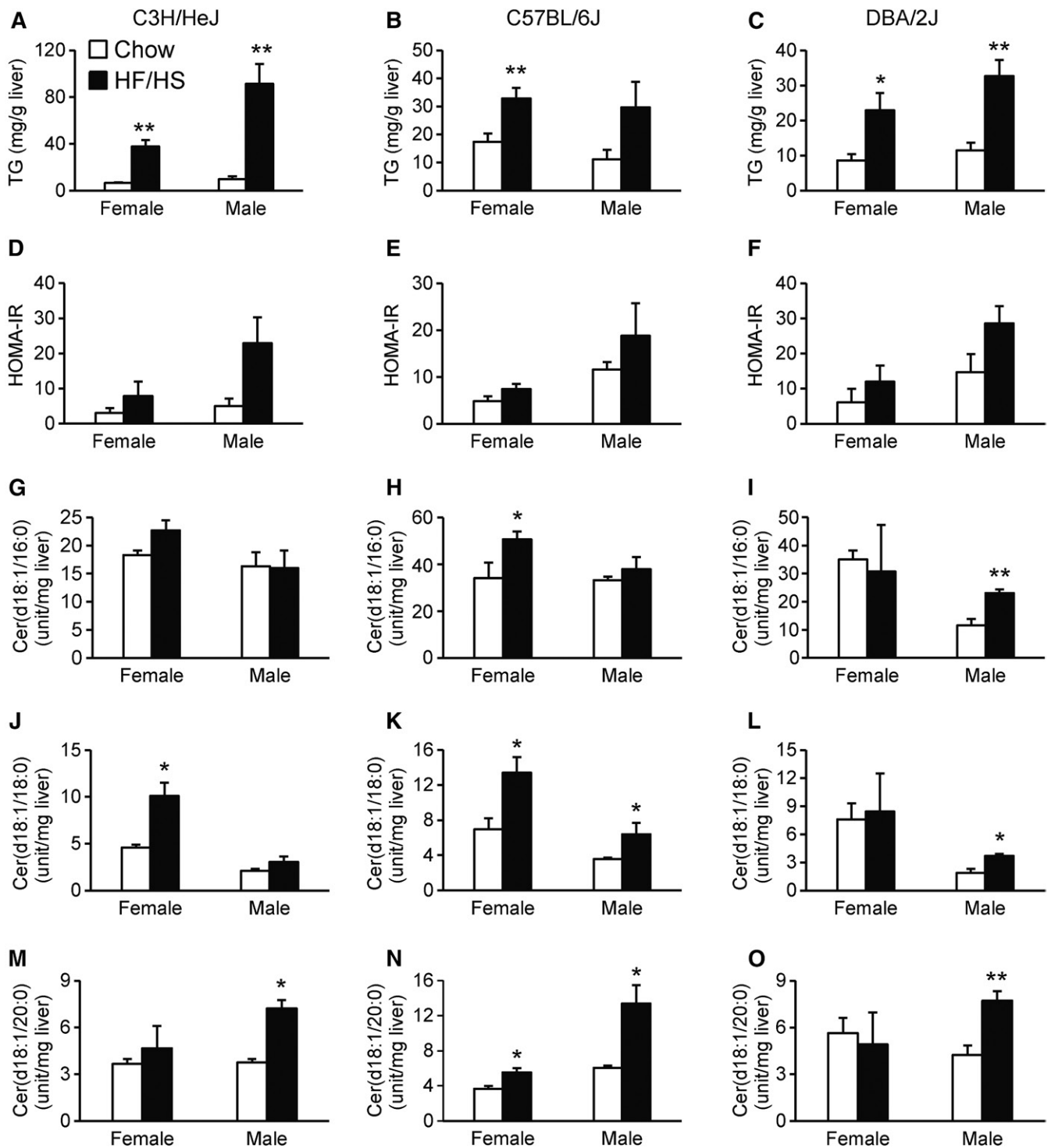


Fig. 3. Effect of HF/HS diet on hepatic ceramide concentration. C3H/HeJ, C57BL/6J, or DBA/2J mice were fed chow (white bars) or HF/HS diets and studied for hepatic TAG (A–C), HOMA-IR (D–F), hepatic Cer(d18:1/16:0) (G–I), hepatic Cer(d18:1/18:0) (J–L), or hepatic Cer(d18:1/20:0) (M–O). The ceramides were measured with HPLC coupled to TOF-MS. Results are presented as means \pm SEM. Statistical differences between groups were tested using unpaired two-tailed Student's *t*-tests. *N* = 3–4 mice per strain, group, and sex. **P* < 0.05 and ***P* < 0.01 between chow and HF/HS fed mice of the same sex and strain.

of hepatic Cer(d18:1/16:0) than mice of the same sex fed a chow diet. Most of the mouse strains of both sexes showed enhanced relative levels of hepatic Cer(d18:1/18:0) on a HF/HS diet (Fig. 3J–L). All the male strains fed a HF/HS diet showed higher relative levels of Cer(d18:1/20:0)

than chow-fed males (Fig. 3M–O). For females, only C57BL/6J mice had significantly more hepatic Cer(d18:1/20:0) on a HF/HS diet (Fig. 3N). These results indicate interaction between sex, diet, and genetics in affecting hepatic ceramides.

Testosterone affects hepatic ceramide synthesis

To evaluate whether gonadal hormones play a role for the sex-difference in hepatic ceramides, we examined the effect of gonadectomy in three inbred strains of mice fed a HF/HS diet for 8 weeks. Gonadectomy increased Cer(d18:1/16:0) and Cer(d18:1/18:0) in all three strains of males (Fig. 4A, C). The increase in Cer(d18:1/16:0) and Cer(d18:1/18:0) was reversed in gonadectomized males with testosterone implants (Fig. 4A, C), although Cer(d18:1/20:0) tended to be reduced in response to gonadectomy in males (Fig. 4E). Testosterone implants significantly increased hepatic Cer(d18:1/20:0) in gonadectomized C3H/HeJ and DBA/2J mice (Fig. 4E). No effect of ovariectomy was observed for Cer(d18:1/16:0) and Cer(d18:1/18:0) in females (Fig. 4B, D). Ovariectomy significantly increased Cer(d18:1/20:0) in female C57BL/6J mice, and tended to increase the relative levels in the two other strains (Fig. 4F).

To determine whether genes encoding enzymes involved in ceramide metabolism (*Sptlc1*, *Sptlc2*, *Cers2*, *Cers4*, *Cers5*, *Cers6*, *Degs1*, *Asah1*, *Ugcg*, *Cerk*, *Kdsr*, and *Smpd1*) were affected by gonadectomy, we compared hepatic expression between sham operated and gonadectomized C57BL/6J mice using mRNA-sequencing (Table 1). Although the mRNA expression levels of *Sptlc1*, *Cers5*, *Cers6*, *Degs1*, *Asah1*, *Ugcg*, and *Kdsr* were higher in females than males, the mRNA expression levels of *Cers2* and *Smpd1* were higher in males than females. The mRNA expression levels of six enzymes (*Sptlc1*, *Cers6*, *Degs1*, *Asah1*, *Cerk*, and *Kdsr*) were significantly increased after gonadectomy in male mice. The expression of *Cers6* was increased the most among the enzymes, and showed more than 2-fold expression after gonadectomy. None of the genes encoding enzymes involved in ceramide metabolism were regulated by ovariectomy in females. To evaluate whether testosterone plays a role in regulating hepatic expression of *Cers6*, we monitored

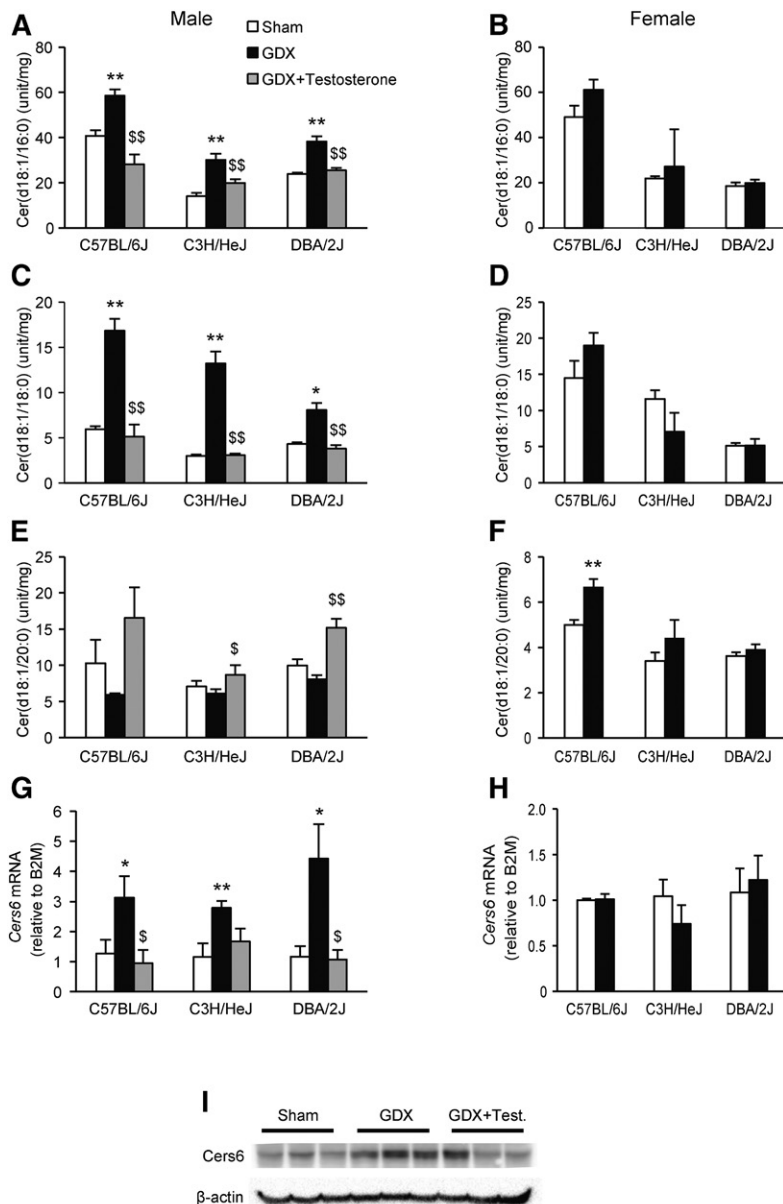


Fig. 4. Gonadectomy increases levels of hepatic Cer(d18:1/16:0) and Cer(d18:1/18:0) in male mice. Hepatic Cer(d18:1/16:0) (A), Cer(d18:1/18:0) (C), and Cer(d18:1/20:0) (E) levels in C57BL/6J, C3H/HeJ, and DBA/2J male mice after gonadectomy (GDX), with or without testosterone implants or sham-operated controls. Hepatic Cer(d18:1/16:0) (B), Cer(d18:1/18:0) (D), and Cer(d18:1/20:0) (F) levels in C57BL/6J, C3H/HeJ, and DBA/2J female mice after ovariectomy (GDX) or sham-operated controls. Hepatic mRNA expression of *Cers6* in male (G), and female (H) mice. The mice were maintained on a chow diet from weaning until 8 weeks of age before switching to a HF/HS diet for another 8 weeks. Results are presented as mean \pm SEM. Statistical differences between groups were tested using unpaired two-tailed Student's *t*-tests ($n = 3-4$ mice per strain, group, and sex). * $P < 0.05$ and ** $P < 0.01$ between the gonadectomized group and sham-operated controls. \$ $P < 0.05$ and \$\$ $P < 0.01$ between gonadectomized males and gonadectomized males with testosterone implants. The ceramides were measured with HPLC coupled to TOF-MS.

TABLE 1. Gonadectomy increases hepatic mRNA levels of several genes encoding enzymes in ceramide metabolism

	Males		Females	
	Sham	GDX	Sham	GDX
<i>Sptlc1</i>	12.7 (0.6)	15.4 (1.0) ^a	15.7 (0.8) ^b	14.4 (0.2)
<i>Sptlc2</i>	15.8 (1.1)	16.8 (0.2)	18.1 (1.5)	19.5 (1.3)
<i>Cers2</i>	230.9 (6.1)	199.5 (7.5) ^c	193.6 (3.6) ^d	194.9 (8.6)
<i>Cers4</i>	2.4 (0.3)	2.5 (0.4)	1.7 (0.3)	2.4 (0.3)
<i>Cers5</i>	1.2 (0.1)	2.1 (0.4)	2.3 (0.3) ^b	2.3 (0.3)
<i>Cers6</i>	10.7 (0.7)	23.5 (1.4) ^e	23.8 (1.5) ^f	23.8 (1.4)
<i>Degs1</i>	48.2 (1.9)	55.2 (1.5) ^a	55.8 (1.1) ^b	52.1 (3.1)
<i>Asah1</i>	23.4 (1.9)	28.5 (0.9) ^a	30.7 (1.8) ^b	32.4 (1.8)
<i>Ugcg</i>	13.8 (0.3)	18.1 (2.3)	21.2 (0.6) ^f	22.1 (1.8)
<i>Cerk</i>	1.9 (0.1)	2.7 (0.2) ^c	2.7 (0.3)	3.0 (0.5)
<i>Kdsr</i>	7.9 (0.2)	12.0 (0.6) ^c	12.3 (0.7) ^d	12.8 (0.6)
<i>Smpd1</i>	25.2 (0.4)	26.1 (0.8)	22.3 (0.1) ^d	25.3 (2.9)

mRNA values are expressed as fragments per kilobase of transcript per million mapped reads (FPKM) (32). Results are presented as mean \pm SEM.

^a $P < 0.05$ between the gonadectomized group and sham-operated controls.

^b $P < 0.05$ between the sexes.

^c $P < 0.01$ between the gonadectomized group and sham-operated controls.

^d $P < 0.01$ between the sexes.

^e $P < 0.001$ between the gonadectomized group and sham-operated controls.

^f $P < 0.001$ between the sexes.

hepatic mRNA expression using qPCR in sham-operated, gonadectomized, and gonadectomized mice with testosterone replacements. Implantation of a testosterone pellet inhibited the increase observed in *Cers6* expression after gonadectomy in all three strains of male mice (Fig. 4G), but not in their female counterparts (Fig. 4H). Finally, we measured *Cers6* protein levels in C57BL/6J sham operated, gonadectomized, and gonadectomized mice with testosterone replacements. *Cers6* protein levels were increased in gonadectomized mice as compared with sham-operated controls (Fig. 4I). Implantation of a testosterone pellet seemed to inhibit the increase observed in *Cers6* protein levels after gonadectomy (Fig. 4I).

Genome-wide association mapping of hepatic ceramides

To investigate differences between the sexes in the control of ceramide metabolism, and to identify genetic loci for hepatic Cer(d18:1/16:0), Cer(d18:1/18:0), and Cer(d18:1/20:0), we performed genome-wide association analyses with $\sim 200,000$ high-quality SNPs spaced throughout the genome. We used a previously determined genome-wide significance threshold of $P = 4.1 \times 10^{-6}$ (8), and corrected for population structure by the mixed model algorithm, FAST-LMM (7). To identify high confidence candidate genes under the LD blocks, we measured global hepatic gene expression and selected genes with both a local expression quantitative trait locus (*cis* eQTL) and a significant correlation between mRNA expression and hepatic ceramide levels or deleterious missense variants.

All the genome-wide significant loci identified for hepatic Cer(d18:1/16:0), Cer(d18:1/18:0), and Cer(d18:1/20:0) were different between sexes (Fig. 5A–F). We identified two genome-wide significant loci for Cer(d18:1/16:0), Cer(d18:1/18:0), and Cer(d18:1/20:0) (Fig. 5A, C, E; Table 2) in females. Whereas one of the loci for Cer(d18:1/18:0) (rs29960779, $P = 1.26 \times 10^{-6}$, Table 2) was the same as identified for Cer(d18:1/16:0), the other

locus was only mapped for Cer(d18:1/18:0) (rs29677623, $P = 3.84 \times 10^{-8}$, Table 2). We identified two genome-wide significant loci associated for Cer(d18:1/18:0) and one genome-wide significant locus for Cer(d18:1/20:0) in males (Table 2). The locus mapped for Cer(d18:1/20:0) at chromosome 2 was the same as identified for Cer(d18:1/18:0) (Table 2). Taken together, our genome-wide association study data demonstrated sex-dependent genetic influence on hepatic ceramide accumulation and shared genetic regulation of certain hepatic ceramide species within sexes.

The chromosome 18 loci for Cer(d18:1/16:0) and Cer(d18:1/18:0) in females were of special interest because only one gene was present within LD for each of them (Fig. 5G, H). Deleted in colorectal cancer (*Dcc*) is the only gene within LD under the peak SNP shared between Cer(d18:1/16:0) and Cer(d18:1/18:0) (rs29960779, $P = 9.05 \times 10^{-8}$, Fig. 5G). The A713V substitution in *Dcc* is predicted to be deleterious for protein function. The only gene within LD under the locus mapped only for Cer(d18:1/18:0) (rs29677623) is neuropilin and tolloid like 1 (*Neto1*) (Fig. 5F). The fact that the expression of *Neto1* is regulated in *cis* ($P = 2.46 \times 10^{-20}$) and has a significant correlation with hepatic Cer(d18:1/18:0) ($r = -0.27$, $P = 0.006$) makes it a likely candidate. *Neto1* also contains an A255T substitution predicted to be deleterious.

DISCUSSION

Mechanistic studies in mice have suggested a causal relationship between ceramides and IR (4–6). Using 98 strains of inbred mice, we show a positive correlation between hepatic concentrations of Cer(d18:1/16:0) and HOMA-IR in both males and females. Hepatic Cer(d18:1/20:0) was associated with IR in male mice only. Males have higher HOMA-IR and hepatic TAG levels than females in our group of inbred mice (9, 11). Thus, it was surprising that

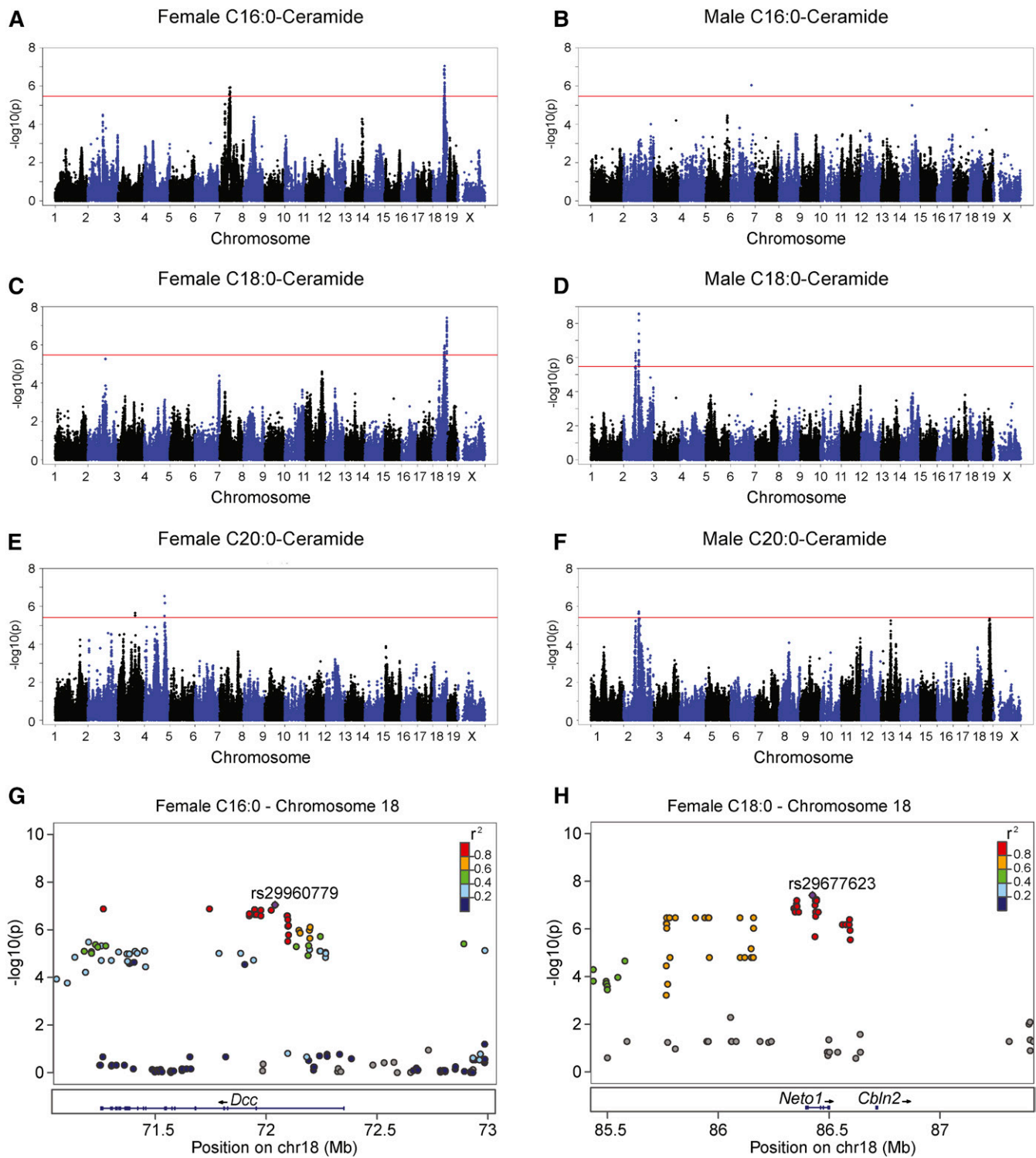


Fig. 5. Genetic control of hepatic Cer(d18:1/16:0) and Cer(d18:1/18:0) in female and male mice. Manhattan plot showing the significance ($-\log_{10}$ of P) of all SNPs and hepatic Cer(d18:1/16:0) (A), Cer(d18:1/18:0) (C), and Cer(d18:1/20:0) (E) after 8 weeks of HF/HS feeding in female mice. Corresponding values for male Cer(d18:1/16:0) (B), Cer(d18:1/18:0) (D), and Cer(d18:1/20:0) (F) after 8 weeks of HF/HS feeding in male mice. Regional plot for genome-wide significant association for hepatic Cer(d18:1/16:0) at chromosome 18 around peak SNP rs29960779 (G). Regional plot for genome-wide significant association for hepatic Cer(d18:1/18:0) on chromosome 18 around peak SNP rs29677623 (H). Pairwise r^2 between the peak SNP and the surrounding SNPs are denoted by color scale.

females generally had higher relative levels of hepatic Cer(d18:1/16:0) and Cer(d18:1/18:0) than their male counterparts. Our data suggest that part of this sex-difference in hepatic ceramide levels can be explained by diet, genetics,

and the inhibitory effect of testosterone on hepatic ceramide synthesis in male mice.

Ceramides may mediate lipid-induced IR (1), and several studies in mice targeting enzymes involved in ceramide

TABLE 2. Genome-wide significant loci for hepatic ceramides in female and male mice

Trait	Sex	Chr.	Peak SNP	Position (Mb)	<i>P</i>	MAF	LD	Number of Genes
C16:0	Female	7	rs31452061	62676830	1.28E-06	0.13	61.4–67.1	33
C16:0	Female	18	rs29960779	72039630	9.05E-08	0.38	71.2–72.1	1
C18:0	Female	18	rs29960779	72039630	1.26E-06	0.38	71.2–72.1	1
C18:0	Female	18	rs29677623	86424649	3.84E-08	0.43	86.1–86.5	1
C18:0	Male	2	rs27994678	75176619	5.35E-07	0.27	74.8–75.6	2
C18:0	Male	2	rs27394020	94055838	2.64E-09	0.19	93.9–94.3	4
C20:0	Male	2	rs27393892	9408751	1.91E-06	0.15	93.9–94.3	6
C20:0	Female	3	rs31152043	1046599257	2.23E-06	0.09	104.6–105.0	9
C20:0	Female	4	rs27552041	123136812	2.85E-07	0.12	123.1–123.2	3


Chr, chromosome; Mb, mega base pairs; MAF, minor allele frequency.

metabolism support a role for ceramides in the development of IR (4–6). However, IR is a complex trait with many factors contributing to impaired insulin action, and the reported impact of hepatic ceramides on insulin sensitivity has been variable (22). Two previous human studies have investigated the relationship between specific hepatic ceramide species and IR (2, 23). Although Luukkonen et al. (2) found a significant correlation between the hepatic concentration of several ceramide species and IR, Ter Horst et al. (23) observed only a trend toward a negative correlation. One explanation for the difference between the studies might be that Luukkonen et al. (2) included more subjects ($n = 125$) in their hepatic ceramide analysis than Ter Horst ($n = 25$) (23). In mice, long-term feeding with a high-fat diet increased hepatic ceramide levels (5). However, feeding C57BL/6J mice a high-fat diet for 7 days induced hepatic IR, but did not increase any of the hepatic ceramide species concentrations (24). Unfortunately, essentially all studies reporting ceramide-induced IR have been conducted in male animals. We now show that increased concentration of hepatic Cer(d18:1/16:0), Cer(d18:1/18:0), and Cer(d18:1/20:0) after 8 weeks of HF/HS diet are strain- and sex-specific. The fact that we observed a significant correlation between Cer(d18:1/16:0) and HOMA-IR, suggests that some of the differences in insulin sensitivity between strains can be explained by differences in hepatic Cer(d18:1/16:0) levels. The male-specific correlations we observed between hepatic Cer(d18:1/20:0) and IR-related phenotypes suggest that Cer(d18:1/20:0) plays sex-specific roles.

Sex-differences in ceramide levels have been reported in heart (25), kidney (26), cerebral cortex (27), and plasma (28, 29). Mielke et al. (28) have shown higher plasma levels of several types of ceramides in females than males. We demonstrate, for the first time, higher levels of hepatic Cer(d18:1/16:0) and Cer(d18:1/18:0) in female than male mice. We also have preliminary data showing higher levels of several types of plasma ceramides in women compared with men (data not shown). Our findings are in accordance with the study conducted by Mielke et al. (28), showing higher levels of different species of plasma ceramides in women than men. Phenotypes including plasma cholesterol and triglycerides, diabetes, and age were correlated with plasma ceramide levels (28). These results highlight the importance of considering sex when studying the relationship between ceramides and chronic disease.

Sex-specific differences can be caused by sex hormones with important roles in the prenatal period, during puberty, and in adults (30). For example, estrogen targets the sphingolipid pathway in breast cancer cells and vascular endothelial cells (31). We report that testosterone suppresses the relative levels of hepatic Cer(d18:1/16:0) and Cer(d18:1/18:0) ceramides in male mice. We also show that testosterone reduces mRNA expression of several genes in ceramide metabolism, including *Cers6*. We finally show that gonadectomy increases *Cers6* protein levels in male mouse livers. Thus, our gonadectomy studies indicate that the sex-difference observed in hepatic Cer(d18:1/16:0) and Cer(d18:1/18:0) is partly due to suppression of *Cers6* by testosterone. Thus, reduced levels of testosterone in elderly men might contribute to the onset of metabolic syndrome.

No previous studies have investigated genetic factors contributing to differences in hepatic ceramide content between individuals. Using a genome-wide association study approach, we identified several significant loci for Cer(d18:1/16:0), Cer(d18:1/18:0), and Cer(d18:1/20:0). All the loci identified for hepatic ceramides are sex-specific. This might not be surprising given the profound impact of testosterone on hepatic Cer(d18:1/16:0) and Cer(d18:1/18:0) in male mice. We found two loci with only one gene within LD: *Dcc* and *Neto1*. To the best of our knowledge, none of these genes have been suggested to impact ceramide levels before.

In conclusion, our data suggest that part of this sex-difference in hepatic ceramide levels can be explained by diet, genetics, and the inhibitory effect of testosterone on hepatic ceramide synthesis in male mice. Whereas our studies support the hypothesis that Cer(d18:1/16:0) affect IR in males as well as females, they reveal novel sex-specific interactions and a potential role of hepatic Cer(d18:1/20:0) for IR. Finally, our findings reinforce the notion that sex is an important biological variable when studying complex traits and disease pathobiology. 

The authors thank Hannah Qi, Zhiqiang Zhou, Judy Wu, and Teyan Han for their expert assistance with mouse experiments, and Sarada Charugundla for plasma metabolite analysis.

REFERENCES

1. Chaurasia, B., and S. A. Summers. 2015. Ceramides - lipotoxic inducers of metabolic disorders. *Trends Endocrinol. Metab.* **26**: 538–550.

2. Luukkonen, P. K., Y. Zhou, S. Sadevirta, M. Leivonen, J. Arola, M. Oresic, T. Hyotylainen, and H. Yki-Jarvinen. 2016. Hepatic ceramides dissociate steatosis and insulin resistance in patients with non-alcoholic fatty liver disease. *J. Hepatol.* **64**: 1167–1175.
3. Holland, W. L., J. T. Brozinick, L. P. Wang, E. D. Hawkins, K. M. Sargent, Y. Liu, K. Narra, K. L. Hoehn, T. A. Knotts, A. Siesky, et al. 2007. Inhibition of ceramide synthesis ameliorates glucocorticoid-, saturated-fat-, and obesity-induced insulin resistance. *Cell Metab.* **5**: 167–179.
4. Xia, J. Y., W. L. Holland, C. M. Kusminski, K. Sun, A. X. Sharma, M. J. Pearson, A. J. Sifuentes, J. G. McDonald, R. Gordillo, and P. E. Scherer. 2015. Targeted induction of ceramide degradation leads to improved systemic metabolism and reduced hepatic steatosis. *Cell Metab.* **22**: 266–278.
5. Turpin, S. M., H. T. Nicholls, D. M. Willmes, A. Mourier, S. Brodesser, C. M. Wunderlich, J. Mauer, E. Xu, P. Hammerschmidt, H. S. Bronnke, et al. 2014. Obesity-induced Cer56-dependent C16:0 ceramide production promotes weight gain and glucose intolerance. *Cell Metab.* **20**: 678–686.
6. Raichur, S., S. T. Wang, P. W. Chan, Y. Li, J. Ching, B. Chaurasia, S. Dogra, M. K. Ohman, K. Takeda, S. Sugii, et al. 2014. CerS2 haploinsufficiency inhibits beta-oxidation and confers susceptibility to diet-induced steatohepatitis and insulin resistance. *Cell Metab.* **20**: 687–695. [Erratum. 2014. *Cell Metab.* **20**: 919.]
7. Parks, B. W., E. Nam, E. Org, E. Kostem, F. Norheim, S. T. Hui, C. Pan, M. Civelek, C. D. Rau, B. J. Bennett, et al. 2013. Genetic control of obesity and gut microbiota composition in response to high-fat, high-sucrose diet in mice. *Cell Metab.* **17**: 141–152.
8. Bennett, B. J., C. R. Farber, L. Orozco, H. M. Kang, A. Ghazalpour, N. Siemers, M. Neubauer, I. Neuhaus, R. Yordanova, B. Guan, et al. 2010. A high-resolution association mapping panel for the dissection of complex traits in mice. *Genome Res.* **20**: 281–290.
9. Parks, B. W., T. Sallam, M. Mehrabian, N. Psychogios, S. T. Hui, F. Norheim, L. W. Castellani, C. D. Rau, C. Pan, J. Phun, et al. 2015. Genetic architecture of insulin resistance in the mouse. *Cell Metab.* **21**: 334–347.
10. Folch, J., M. Lees, and G. H. Sloane Stanley. 1957. A simple method for the isolation and purification of total lipides from animal tissues. *J. Biol. Chem.* **226**: 497–509.
11. Norheim, F., S. T. Hui, E. Kulahcioglu, M. Mehrabian, R. M. Cantor, C. Pan, B. W. Parks, and A. J. Lusis. 2017. Genetic and hormonal control of hepatic steatosis in female and male mice. *J. Lipid Res.* **58**: 178–187.
12. Hsu, F. F., and J. Turk. 2000. Structural determination of sphingomyelin by tandem mass spectrometry with electrospray ionization. *J. Am. Soc. Mass Spectrom.* **11**: 437–449.
13. Castellani, L. W., C. N. Nguyen, S. Charugundla, M. M. Weinstein, C. X. Doan, W. S. Blaner, N. Wongsiriroj, and A. J. Lusis. 2008. Apolipoprotein AII is a regulator of very low density lipoprotein metabolism and insulin resistance. *J. Biol. Chem.* **283**: 11633–11644.
14. Hui, S. T., B. W. Parks, E. Org, F. Norheim, N. Che, C. Pan, L. W. Castellani, S. Charugundla, D. L. Dirks, N. Psychogios, et al. 2015. The genetic architecture of NAFLD among inbred strains of mice. *eLife.* **4**: e05607.
15. Dobin, A., C. A. Davis, F. Schlesinger, J. Drenkow, C. Zaleski, S. Jha, P. Batut, M. Chaisson, and T. R. Gingeras. 2013. STAR: ultrafast universal RNA-seq aligner. *Bioinformatics.* **29**: 15–21.
16. Seldin, M. M., Y. Meng, H. Qi, W. Zhu, Z. Wang, S. L. Hazen, A. J. Lusis, and D. M. Shih. 2016. Trimethylamine N-oxide promotes vascular inflammation through signaling of mitogen-activated protein kinase and nuclear factor- κ B. *J. Am. Heart Assoc.* **5**: e002767.
17. Hevener, A. L., W. He, Y. Barak, J. Le, G. Bandyopadhyay, P. Olson, J. Wilkes, R. M. Evans, and J. Olefsky. 2003. Muscle-specific Pparg deletion causes insulin resistance. *Nat. Med.* **9**: 1491–1497.
18. Hevener, A. L., J. M. Olefsky, D. Reichart, M. T. Nguyen, G. Bandyopadhyay, H. Y. Leung, M. J. Watt, C. Benner, M. A. Febbraio, A. K. Nguyen, et al. 2007. Macrophage PPAR gamma is required for normal skeletal muscle and hepatic insulin sensitivity and full anti-diabetic effects of thiazolidinediones. *J. Clin. Invest.* **117**: 1658–1669.
19. Steele, R. 1959. Influences of glucose loading and of injected insulin on hepatic glucose output. *Ann. N. Y. Acad. Sci.* **82**: 420–430.
20. Yang, H., Y. Ding, L. N. Hutchins, J. Szatkiewicz, T. A. Bell, B. J. Paigen, J. H. Graber, F. P. de Villena, and G. A. Churchill. 2009. A customized and versatile high-density genotyping array for the mouse. *Nat. Methods.* **6**: 663–666.
21. Lippert, C., J. Listgarten, Y. Liu, C. M. Kadie, R. I. Davidson, and D. Heckerman. 2011. FaST linear mixed models for genome-wide association studies. *Nat. Methods.* **8**: 833–835.
22. Petersen, M. C., and G. I. Shulman. 2017. Roles of diacylglycerols and ceramides in hepatic insulin resistance. *Trends Pharmacol. Sci.* **38**: 649–665.
23. Ter Horst, K. W., P. W. Giljames, R. I. Versteeg, M. T. Ackermans, A. J. Nederveen, S. E. la Fleur, J. A. Romijn, M. Nieuworp, D. Zhang, V. T. Samuel, et al. 2017. Hepatic diacylglycerol-associated protein kinase epsilon translocation links hepatic steatosis to hepatic insulin resistance in humans. *Cell Reports.* **19**: 1997–2004.
24. Turner, N., G. M. Kowalski, S. J. Leslie, S. Risis, C. Yang, R. S. Lee-Young, J. R. Babb, P. J. Meikle, G. I. Lancaster, D. C. Henstridge, et al. 2013. Distinct patterns of tissue-specific lipid accumulation during the induction of insulin resistance in mice by high-fat feeding. *Diabetologia.* **56**: 1638–1648.
25. Kadokami, T., C. F. McTiernan, T. Kubota, C. S. Frye, and A. M. Feldman. 2000. Sex-related survival differences in murine cardiomyopathy are associated with differences in TNF-receptor expression. *J. Clin. Invest.* **106**: 589–597.
26. Durant, B., S. Forni, L. Sweetman, N. Brignol, X. L. Meng, E. R. Benjamin, R. Schiffrin, and J. S. Shen. 2011. Sex differences of urinary and kidney globotriaosylceramide and lyso-globotriaosylceramide in Fabry mice. *J. Lipid Res.* **52**: 1742–1746.
27. Barrier, L., S. Ingrand, B. Fauconneau, and G. Page. 2010. Gender-dependent accumulation of ceramides in the cerebral cortex of the APP(SL)/PS1Ki mouse model of Alzheimer's disease. *Neurobiol. Aging.* **31**: 1843–1853.
28. Mielke, M. M., V. V. Bandaru, D. Han, Y. An, S. M. Resnick, L. Ferrucci, and N. J. Haughey. 2015. Demographic and clinical variables affecting mid- to late-life trajectories of plasma ceramide and dihydroceramide species. *Aging Cell.* **14**: 1014–1023.
29. Weir, J. M., G. Wong, C. K. Barlow, M. A. Greeve, A. Kowalczyk, L. Almasy, A. G. Comuzzie, M. C. Mahaney, J. B. Jowett, J. Shaw, et al. 2013. Plasma lipid profiling in a large population-based cohort. *J. Lipid Res.* **54**: 2898–2908.
30. Mauvais-Jarvis, F. 2015. Sex differences in metabolic homeostasis, diabetes, and obesity. *Biol. Sex Differ.* **6**: 14.
31. Sukocheva, O., C. Wadham, and P. Xia. 2009. Role of sphingolipids in the cytoplasmic signaling of estrogens. *Steroids.* **74**: 562–567.
32. Trapnell, C., A. Roberts, L. Goff, G. Pertea, D. Kim, D. R. Kelley, H. Pimental, S. L. Salzberg, J. L. Rinn, and L. Pachter. 2012. Differential gene and transcript expression analysis of RNA-seq experiments with TopHat and Cufflinks. *Nat. Protoc.* **7**: 562–578.